Comparative Anatomy of the Mammalian Corneal Subbasal Nerve Plexus

Carl Marfurt,[1] Miracle C. Anokwute,[1] Kaleigh Fetcko,[1] Erin Mahony-Perez,[1] Hassan Farooq,[1] Emily Ross,[1] Maraya M. Baumanis,[1] Rachel L. Weinberg,[2] Megan E. McCarron,[2] and Joseph L. Mankowski[2]

[1]Indiana University School of Medicine-Northwest-Gary, Gary, Indiana, United States
[2]Johns Hopkins University School of Medicine, Baltimore, Maryland, United States

Correspondence: Carl Marfurt, Department of Anatomy, Cell Biology and Physiology, Indiana University School of Medicine-Northwest-Gary, 3400 Broadway, Gary, IN 46408, USA;
cmarfurt@iun.edu.

Submitted: September 25, 2019
Accepted: October 24, 2019

Citation: Marfurt C, Anokwute MC, Fetcko K, et al. Comparative anatomy of the mammalian corneal subbasal nerve plexus. *Invest Ophthalmol Vis Sci*. 2019;60:4972–4984. https://doi.org/10.1167/iovs.19-28519

Purpose. The subbasal nerve plexus (SNP) is the densest and most recognizable component of the mammalian corneal innervation; however, the anatomical configuration of the SNP in most animal models remains incompletely described. The purpose of the current study is to describe in detail the SNP architecture in eight different mammals, including several popular animal models used in cornea research.

Methods. Corneal nerves in mouse, rat, guinea pig, rabbit, dog, macaque, domestic pig, and cow eyes were stained immunohistochemically with antiserum directed against neurotubulin. SNP architecture was documented by digital photomicrography and large-scale reconstructions, that is, corneal nerve maps, using a drawing tube attached to a light microscope.

Results. Subbasal nerve fibers (SNFs) in mice, rats, guinea pigs, dogs, and macaques radiated centrally from the corneoscleral limbus toward the corneal apex in a whorl-like or spiraling pattern. SNFs in rabbit and bovine corneas swept horizontally across the ocular surface in a temporal-to-nasal direction and converged on the inferonasal limbus without forming a spiral. SNFs in the pig cornea radiated centrifugally in all directions, like a starburst, from a focal point located equidistant between the corneal apex and the superior pole.

Conclusions. The results of the present study have demonstrated for the first time substantial interspecies differences in the architectural organization of the mammalian SNP. The physiological significance of these different patterns and the mechanisms that regulate SNP pattern formation in the mammalian cornea remain incompletely understood and warrant additional investigation.

Keywords: corneal innervation, corneal nerves, subbasal nerves, trigeminal nerve, ocular nerves

The mammalian cornea is the most densely innervated surface tissue in the body. In addition to their important sensory functions, corneal nerves help maintain a healthy ocular surface by releasing trophic neuropeptides that promote corneal epithelial homeostasis and by activating brainstem circuits that promote reflex blinking and lacrimation.

Anatomically, the corneal innervation in most mammals is organized into four main layers: mid-stromal nerves, subepithelial plexus, subbasal nerve plexus (SNP), and intraepithelial nerve terminals.[1–3] The SNP is the densest and most recognizable layer of the corneal innervation and is an important morphologic landmark. The SNP is made up of large numbers of individual subbasal nerve fibers (SNFs), each with a highly characteristic morphologic appearance and running parallel to one another within a very narrow plane of focus. The term "subbasal" is a misnomer that is deeply entrenched in the literature. The term derives from early anatomical studies of the mammalian corneal innervation in which investigators concluded, mistakenly, that the subbasal nerves were located beneath the epithelial basal lamina.[4,5] Subsequent ultrastructural studies[6,7] have demonstrated unequivocally that the SNFs are situated, in actuality, in the deep, subnuclear region of the basal epithelial cell layer, either between the basal epithelial cells and their basal lamina, or within cytoplasmic infoldings of the basal epithelial cell membranes. SNFs in human[8–12] and animal[13–19] corneas are readily imaged by in vivo confocal microscopy (IVCM), and changes in SNF density and morphology have been quantified to assess the status of the corneal innervation in a variety of diseases and postoperative conditions.

The murine model is used extensively in corneal nerve research due to the similarity of the mouse genome to that of humans and because many different murine transgenic and knockout strains are available. Not surprisingly, the anatomy of mouse corneal innervation has received considerable attention and is well described.[3,20] SNPs in human and mouse corneas are comparable. In both species, SNFs radiate centripetally from the corneoscleral limbus in a characteristic whorl-like or spiral-like configuration.[2,3,21] On the basis of these observations, it is often assumed that a whorl-like assemblage of SNFs is a ubiquitous feature of all mammalian corneas; however, the architectural organization of the SNP in many popular animal models of corneal research has not been investigated or remains incompletely described.

Detailed knowledge of mammalian SNP architecture is essential because following injury to the corneal innervation

Table 1. Animal Corneas Used in This Study

Species	Strain or Breed	Number of Corneas	Sources of Animals	Method of Euthanasia
Mouse	C57BL/6 and BALB/c	49	Commercial vendor	CO_2 inhalation
Rat	Sprague-Dawley	75	Commercial vendor	Sodium pentobarbital, intraperitoneal
Guinea Pig	Dunkin Hartley	10	Commercial vendor	Sodium pentobarbital, intraperitoneal
Rabbit	New Zealand White	8	Commercial vendor	Sleepaway euthanasia solution, intravenous
Dog	Mixed breeds	3	Gift from Chris J. Murphy, DVM, PhD, UC Davis; dogs euthanized for medical reasons unrelated to current study	Sleepaway euthanasia solution, intravenous
Macaque	Pigtailed (*Macaca nemestrima*, $n = 23$) and rhesus (*Macaca mulatta*, $n = 3$)	26	Johns Hopkins University	Sodium pentobarbital, intravenous
Domestic Pig	Hampshire, American Yorkshire	8	Local slaughterhouse	Approved methods
Cow	Angus	8	Local slaughterhouse	Approved methods

by trauma, disease, or surgery, corneal nerve regeneration takes place primarily through sprouting and elongation of damaged and intact SNFs.[22–25] The efficacy of corneal nerve regeneration in animal models is generally assessed quantitatively by evaluating changes in SNF density, rate of elongation, and morphology over time.[26] In addition, longitudinal studies of SNP density are used to monitor the success of pharmacologic and other therapeutic interventions on diseases affecting corneal nerves.[27]

The purpose of the current immunohistochemical (IHC) investigation was to describe in detail the SNP architecture in eight different mammals, including several that are popular animal models for corneal nerve research: the mouse, rat, guinea pig, rabbit, dog, macaque, domestic pig, and cow. This study revealed three distinct patterns of SNF organization, disproving the conception that SNP architecture is identical in all mammalian corneas. In some mammals, SNFs project centripetally and form a gentle whorl-like pattern that converges in the periapical cornea as a spiral or vortex. In other mammals, SNFs sweep horizontally across the ocular surface in a temporal-to-nasal direction and converge on the inferonasal limbus without forming a spiral. In still other mammals, the SNP consists of SNFs that radiate centrifugally in all directions from a focal point located between the corneal apex and the superior pole of the eye.

Materials and Methods

Corneal Harvesting and Tissue Preparation

A total of 183 whole corneas from eight different mammalian species were used in the current investigation. The strain, source, method of euthanasia, and number of corneas examined for each species is given in Table 1. All animals were treated in accordance with the ARVO Statement for the Use of Animals in Ophthalmic and Vision Research and all procedures involving animals were approved by the Institutional Animal Care and Use Committees of Indiana University School of Medicine-Northwest-Gary and Johns Hopkins University.

Mouse, rat, guinea pig, and rabbit eyes were oriented prior to enucleation by placing an indelible ink mark at the superior limbus. The globes were removed whole and immersion-fixed for 15 to 20 minutes in room temperature (RT) 4% paraformaldehyde in 0.1 M phosphate-buffered saline (PBS), pH 7.3. The corneas were then dissected free and immersion-fixed for either an additional 1 hour (mice, rats, and guinea pigs) or 12 to 24 hours (rabbits). Canine corneas were dissected free within 1 hour of death; each cornea was oriented by placing a suture at the superior limbus prior to harvesting and were then immersion-fixed for 1 to 2 weeks in ice cold 4% paraformaldehyde. Macaque corneas were removed with an 8-mm trephine and immersion-fixed overnight in cold 10% neutral buffered formalin. Bovine and porcine eyes were enucleated 2 to 10 hours after death, and the entire globes were immersion-fixed for 1 to 2 days in RT 4% paraformaldehyde in 0.1 M PBS, after which the corneas were dissected free and immersion-fixed for an additional 1 to 2 days at 4°C. Mouse, macaque, cow, and pig eyes were not oriented prior to harvesting; however, directionality in the latter two species was determined postmortem by referencing the nasomedial position of the nictitating membrane. Following immersion fixation, all corneas from all species were transferred into ice cold 0.1 M PBS containing 30% wt/vol sucrose and stored until they could be processed.

Methodological processing of corneas prior to IHC staining was customized in accordance with interspecies differences in corneal size and thickness. In most animals with relatively small and thin corneas (mice, rats, and guinea pigs), four radial slits were made with a razor blade from the limbus to within ~1 mm of the corneal apex to produce "clover-leaf" preparations. The specimens were then processed for IHC staining as free-floating whole mounts. Most of the larger mammalian corneas (rabbits, dogs, pigs, and cows) were cut into three or four pieces using one of two methods. In the majority of cases, a 6.0-mm diameter central corneal button was removed with a trephine and the peripheral cornea was then cut into nasal and temporal halves (rabbits and dogs) or four quadrants (pigs and cows). In a few cow corneas, the corneas were cut into quadrants without first removing a central button. For each of the macaque corneas, a central 5-mm diameter button was removed with a biopsy punch and processed as a whole mount.

To facilitate IHC staining of the SNFs in rabbit, dog, pig, and cow corneas, the corneal epithelium and subepithelial stroma were isolated from the posterior portion of the cornea. Under a dissecting microscope, a small slit was made along the lateral edge of the stroma with a #11 scalpel blade approximately 150 to 300 μm beneath the anterior corneal surface. The anterior portion of the cornea was then isolated by pulling firmly along this fracture line with a microforceps. The specimen was then pressed onto a smooth foundation of frozen optimal cutting temperature (OCT) compound and multiple 40-μm thick

Investigative Ophthalmology & Visual Science

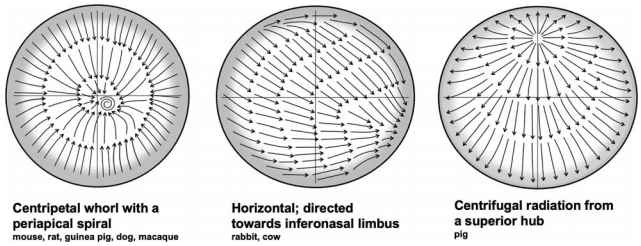

Figure 1. Schematic illustration depicting the three main patterns of mammalian SNP architecture observed in this study. *Arrows* indicate direction of SNF orientation.

frozen sections were taken from the posterior surface of the specimen using a cryostat. Sectioning was then halted and the residual corneal specimen, consisting of the entire corneal epithelium and approximately 50 to 100 μm of superficial stroma, was released from the frozen OCT matrix by thawing in ice cold PBS.

IHC Staining

To enhance tissue permeability and optimize IHC staining, corneas from all animals except mice were first permeabilized in 0.01% hyaluronidase (type IV-S, catalogue #H4272, Sigma-Aldrich, Corp., St. Louis, MO, USA) and 0.1% ethylenediaminetetraacetic acid (EDTA) (catalogue #E5391, Sigma-Aldrich, Corp.) in 0.1 M PBS, pH 5.3.[28] Rat and guinea pig corneas were incubated in the permeability reagent overnight at RT, whereas corneas from all larger mammals were incubated for 24 to 48 hours at 37°C. Mouse corneas were permeabilized prior to fixation with 2% TritonX-100 in 0.1 M PBS at RT for 10 to 15 minutes.

All tissues were then rinsed three times for 20 minutes each in PBS + 0.3% Triton X-100 (PBS-TX), incubated for 2 hours in blocking serum (1% bovine serum albumin in PBS-TX) and incubated for 4 days (macaques) or overnight (all other species) at RT on a rocker table in either a rabbit polyclonal antibody (mouse corneas) or a mouse monoclonal antibody (all other corneas) against neuronal class III β-tubulin (TuJ1, 1:500, Covance Research Products, Berkeley, CA, USA). After three more PBS-TX rinses, the tissues were incubated for 2 hours at RT in an appropriate secondary antibody (biotinylated anti-rabbit or anti-mouse IgG, 1:200; Vector Laboratories, Burlingame, CA, USA), rinsed three times in PBS-TX, and incubated for 2 hours at RT in avidin-biotin-horseradish peroxidase complex (ABC reagent; Vector Laboratories). The tissues were rinsed three more times in PBS-TX and then incubated for 8 minutes at RT in 0.1% diaminobenzidine (Sigma-Aldrich Corp.) and 0.009% H_20_2 followed by three more rinses each in PBS and distilled water. They were then air-dried on chrome alum-gelatin coated slides, dehydrated in graded alcohols, and coverslipped with Permount under weighted coverslips.

All specimens were examined in a Leica DM4000 research microscope equipped with brightfield and darkfield condensers. Digital images of the immunohistochemically stained SNFs were captured with a Leica DFC420C camera and photomontages were assembled using the merge tool of Adobe Photoshop. Detailed schematic line drawings of select areas of the SNP were prepared at final magnifications of 155× or 310× by attaching a drawing tube to the light microscope. Although labeled nerves were observed throughout all layers of the corneal epithelium and stroma, for the purposes of this investigation only SNFs were illustrated using the drawing tube.

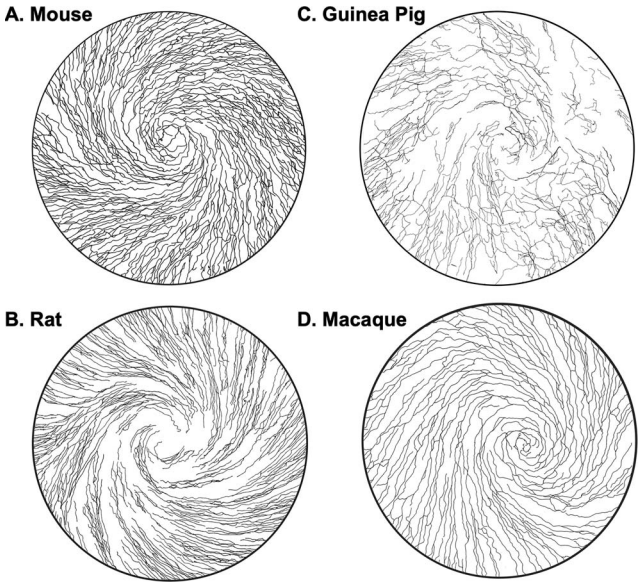

Figure 2. *Line drawings* showing the morphological appearances of SNP spirals in representative mouse (**A**), rat (**B**), guinea pig (**C**), and macaque (**D**) corneas. The diameters of the corneal areas illustrated are 0.5 mm for the mouse, 1.0 mm for the rat and guinea pig, and 1.5 mm for the macaque.

Results

Summary of Main Findings

The results of this study of SNP architecture in eight different mammals demonstrated three distinctive patterns of SNP organization (Fig. 1). The SNP in mice, rats, guinea pigs, dogs, and macaques contained SNFs that radiated centripetally from the corneoscleral limbus toward the corneal apex in a whorl-like or spiraling pattern. The SNP in rabbits and cows was composed of SNFs that swept across the corneal surface in a roughly horizontal, temporal-to-nasal direction. The fibers were oriented preferentially toward the inferonasal limbus and did not form a spiral. The SNP in pigs consisted of SNFs that radiated centrifugally in all directions from a focal point located along the vertical meridian partway between the corneal apex and the superior pole of the cornea.

Mammals in Which the SNP Forms a Centripetal Whorl-like Pattern

In five of the species examined in this study, the mouse, rat, guinea pig, dog, and macaque, the SNP formed a highly organized, centripetally directed whorl-like pattern. Close to the corneal apex, the SNP in the majority of mice, rats, and guinea pigs (90.1%, 63.2%, and 60.0%, respectively) and in 100% of the macaques ended as a conspicuous logarithmic spiral or vortex (Figs. 2, 3). A pronounced spiral pattern was especially well-developed in mice and macaque corneas (Fig. 4). In a smaller percentage of mice, rats, and guinea pigs, SNFs did not form a terminal spiral and converged in a roughly symmetric fashion about an imaginary focal point, on opposing sides of an imaginary linear seam, or some combination of the above ("mixed pattern") (Figs. 5, 6).

In mice and rat corneas with prominent SNF spirals, a slight majority (59.4% and 56.3%, respectively) rotated in the clockwise direction (Fig. 7). In macaques, 65.3% of the spirals

Investigative Ophthalmology & Visual Science

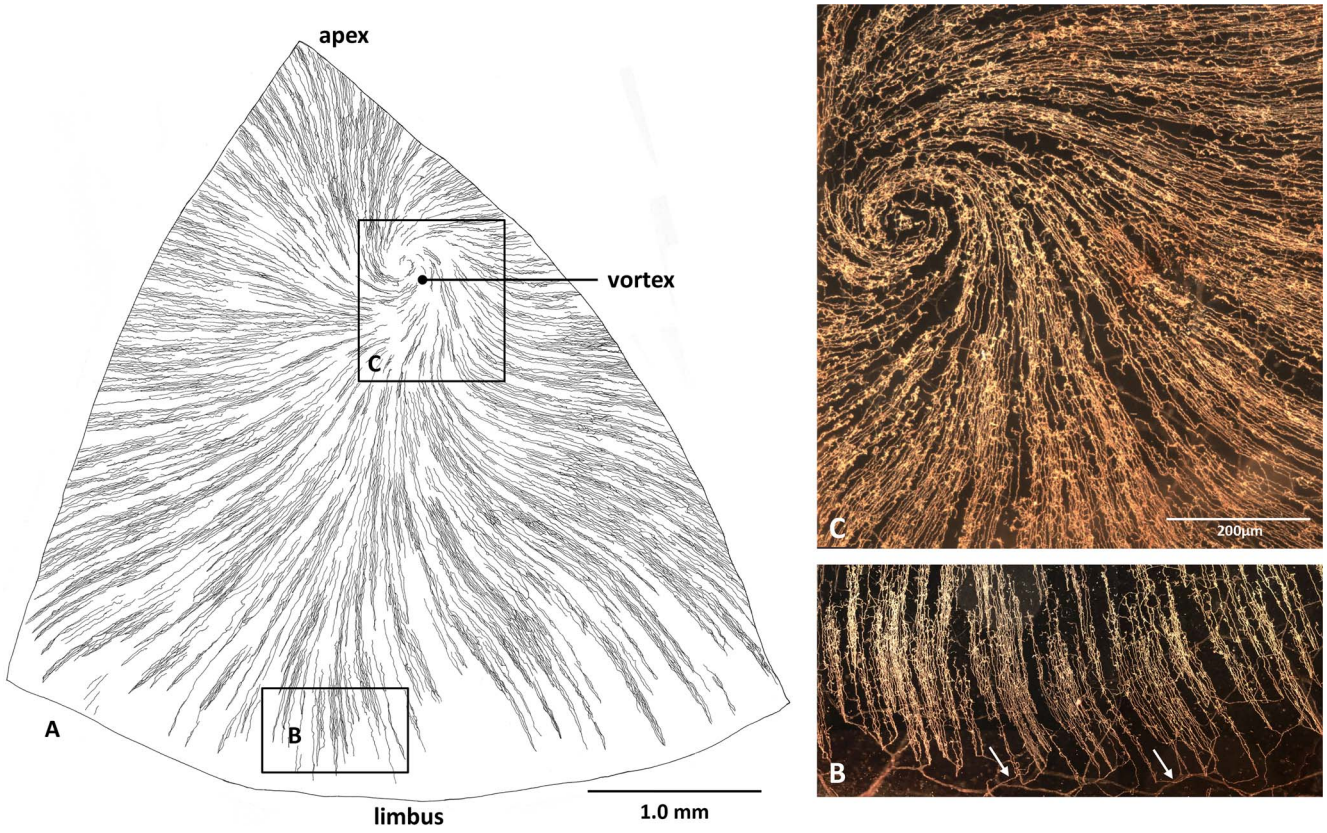

FIGURE 3. Rat corneal SNP. (**A**) *Line drawing* showing the density and directional orientations of SNFs in the inferonasal quadrant of a representative rat cornea. (**B, C**) Darkfield photomicrographs reveal SNP morphology in areas similar to those enclosed by the *inset boxes* in **A**. (**B**) In the extreme peripheral cornea, assemblages of SNFs known as "epithelial leashes" take origin from superficial stromal nerves (*arrows*) and project radially or in a curvilinear fashion toward the central cornea. (**C**) SNFs sweep uniformly toward the periapical region where they converge to form a spiral or vortex.

rotated counterclockwise, whereas in guinea pigs 50% rotated clockwise and the other 50% rotated counterclockwise. There was no correlation between ocular sidedness (left or right eye) and directionality of the spiral; in many animals with bilateral spirals, the whorls rotated in opposite directions. The epicenter of SNF convergence in rat corneas was located most frequently inferonasal (63.4%) or superonasal (33.8%) to the corneal apex; in guinea pigs, the epicenter was located either inferonasal to the apex (80.0%) or centered precisely on the corneal apex (20%), and in dogs the epicenter was located inferotemporal to the apex. The precise epicenters of the mouse and macaque SNP whorls were not determined in this investigation because the corneas in these species were not oriented prior to enucleation. Three of the C57BL/6 mouse corneas examined in this study contained multiple spirals (i.e., two doubles and one triplet) (Fig. 8); all other mammalian corneas examined in this study possessed only a single spiral.

IHC staining of the SNP in the three dog corneas examined in this study was incomplete due to inconsistent labeling of SNFs in the apical corneal zone. SNFs in the peripheral and paracentral canine cornea stained extremely well and revealed, even in the absence of data from the apical cornea, a conspicuous centripetal convergence pattern (Fig. 9). In all three cases, the whorl-like assemblages of dog SNFs converged on a location slightly inferotemporal to the corneal apex.

Mammals in Which the SNP Does Not Form a Centripetal Whorl-like Pattern

In rabbit and cow corneas, SNFs did not form a centripetal whorl but instead swept across the corneal epithelium in a largely horizontal, temporal-to-nasal direction with the vast majority of fibers oriented uniformly toward the inferonasal limbus (Figs. 10, 11). The SNP patterns in these two species were similar; however, the overall innervation density of the cow eye (not illustrated) was lower, and bovine epithelial leashes tended to course largely independent of one another and anastomosed infrequently with neighboring SNFs.

SNFs in pig corneas coursed centrifugally from an imaginary focal point located along the vertical meridian, approximately one-third of the distance between the superior pole and the corneal apex (Fig. 12). At the epicenter of the focal point, the SNP consisted of a delicate network of anastomotic fibers; the latter network then quickly transitioned around the margins into more "typical" SNFs that radiated centrifugally, like a starburst, in every direction toward the corneoscleral limbus (Fig. 13).

Nerve Orientations Near the Corneoscleral Limbus

In some of the guinea pig, rabbit, and dog corneas examined in this study, SNFs and/or their intraepithelial terminals in the extreme peripheral cornea often coursed preferentially toward the limbus (Fig. 14). In many of these locations, the strong

Investigative Ophthalmology & Visual Science

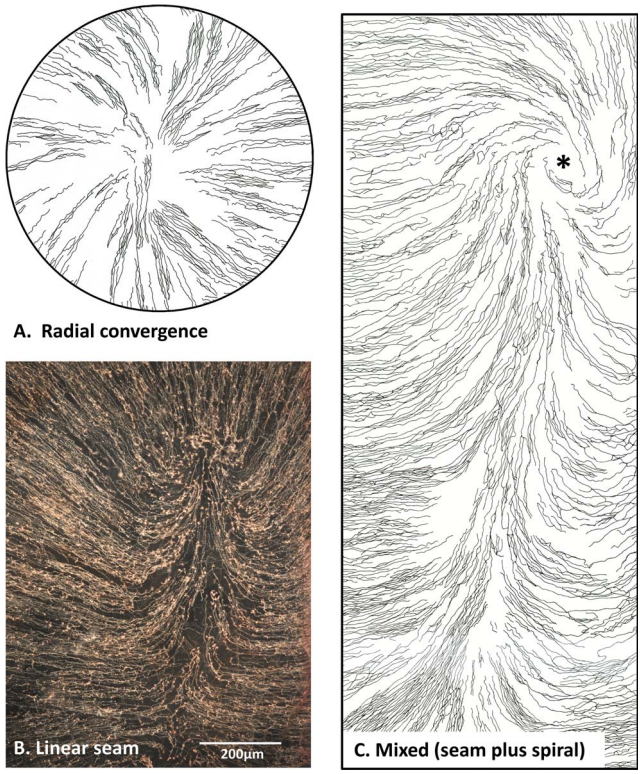

FIGURE 4. "Nonspiral" central SNF convergence patterns in rat corneas. (**A**) Radially symmetric convergence. (**B**) Convergence on opposite sides of an imaginary seam. (**C**) Mixed pattern. In the mixed pattern shown here, SNFs converge on opposing sides of a nearly 2-mm-long linear seam that transitions, closer to the apex, into a small vortex (*asterisk*). Figure **A** is 1.0 mm in diameter and **C** is 2.5 × 1.0 mm.

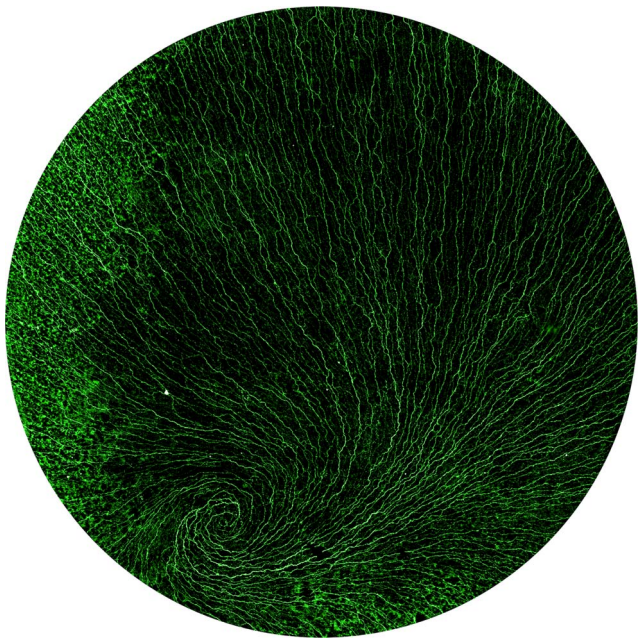

FIGURE 5. SNFs in a pigtailed macaque cornea. As the nerve fibers converge they form a highly regular, clockwise logarithmic spiral. The diameter of the corneal central plug is 5.0 mm and the nerve fibers have been pseudo-colorized.

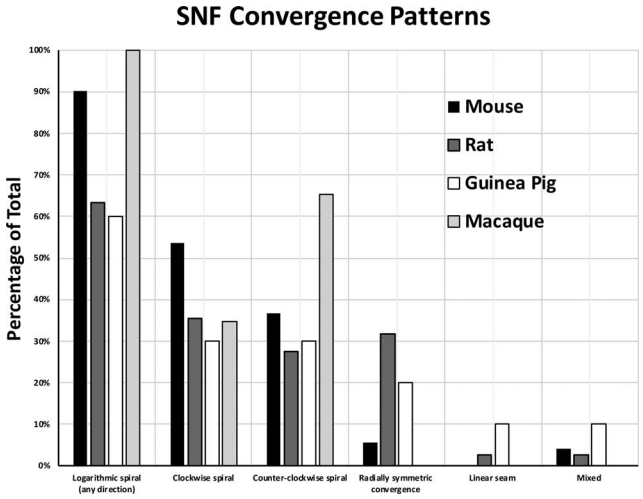

FIGURE 6. *Bar graph* showing the percentages of mouse, rat, guinea pig, and macaque corneas that display a particular SNF convergence pattern.

directional SNF bias toward the limbus was diametrically opposed to the prevailing directional orientation of the SNP as a whole.

DISCUSSION

This study demonstrated significant interspecies differences in mammalian SNP architecture. Three distinct patterns of SNF organization are recognized. In mouse, rat, guinea pig, dog, and macaque corneas, the SNFs form a dense, whorl-like pattern that converges on the periapical cornea in most cases as a conspicuous spiral or vortex. In rabbit and bovine corneas, SNFs sweep horizontally across the ocular surface in a temporal-to-nasal direction. In domestic pigs, SNFs radiate centrifugally from a focal point located along the vertical meridian part-way between the corneal apex and the superior pole.

Mammals in Which the SNP Forms a Whorl-like Pattern

The results of the present study confirm and extend prior reports of whorl-like assemblages of corneal SNFs in the mouse,[3,20,29–40] rat,[22,41,42] and macaque.[43] SNP whorl-like patterns have also been reported in human[2,21,24,44–50] and cat[51] corneas. The results of the present study now add two additional species to this list: guinea pig and dog. Overall, whorl-like patterns occur in the majority (7 of 11, or 63.6%) of mammalian species for which data are currently available (Table 2).

The mechanisms that govern the formation and maintenance of whorl-like arrangements of SNFs remain poorly understood. According to the XYZ hypothesis of corneal epithelial renewal,[52] basal epithelial cells near the corneoscleral limbus divide and migrate centripetally in a whorl-like fashion toward the corneal apex in response to chemotropic guidance, electromagnetic cues, population pressures, and preferential desquamation of central epithelial cells.[53–61] As the basal epithelial cells slide continuously toward the corneal apex, SNFs lodged within narrow intercellular spaces between adjacent columns of migrating cells or sequestered within cytoplasmic infoldings of these cells[6,7,62] are pulled along and guided into analogous curvilinear patterns.[30,63] As the nerves and epithelial cells approach the corneal apex, some unknown

Investigative Ophthalmology & Visual Science

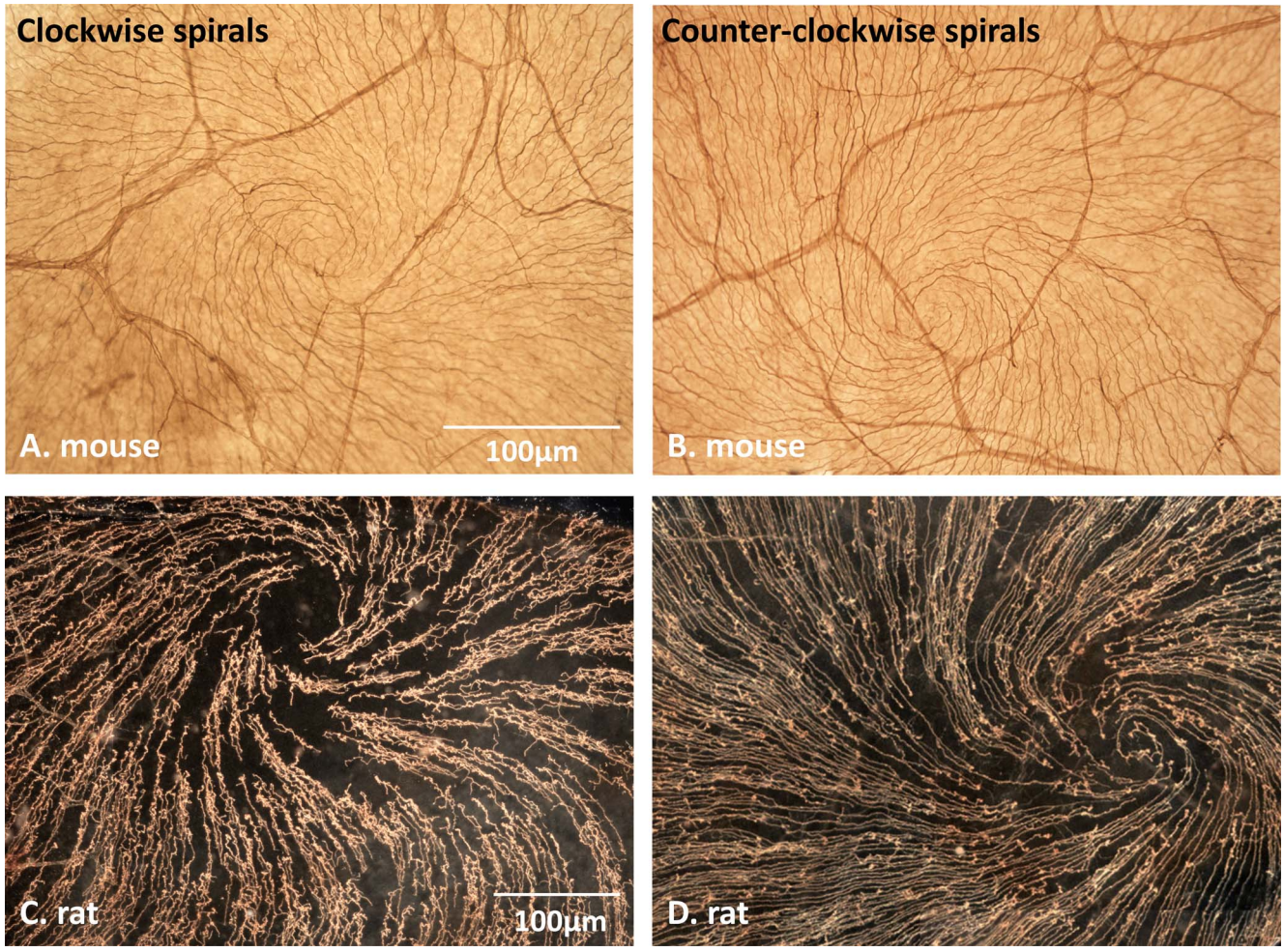

Figure 7. Photomicrographs showing clockwise (**A, C**) and counterclockwise (**B, D**) SNF spiral rotations in rodent corneas. The calibration bar in **A** applies to both mouse corneas, and the calibration bar in **B** applies to both rat corneas.

force, perhaps a tangential electric force or magnetic field directed perpendicular to the centripetal direction of migration, compels them to arch sideways into a spiral pattern.[60]

The whorl-like pattern seen in most mammalian corneas is reminiscent of a logarithmic or Fibonacci spiral, a growth pattern found ubiquitously in nature in rapidly growing plants.[64] Whorl-like patterns of hair follicles are seen also on the vertex of the human scalp[65,66] and on the faces and bodies of horses.[67] Human scalp whorls are thought to result from increased tension on the epidermis during rapid expansion of the cranium,[67] a situation analogous perhaps to the developing cornea where stress and mechanical forces related to rapid eye growth and intraocular pressure may have consequences for nerve pattern formation.[61]

Not all evidence supports a causal relationship between epithelial cell migration and SNP pattern formation. Studies in the developing mouse cornea show that SNF whorl formations are first observed at approximately 3 to 4 weeks postpartum; however, basal epithelial cell whorl formations do not develop until 4 to 8 weeks after birth.[3,31,34,58,60,68] These findings

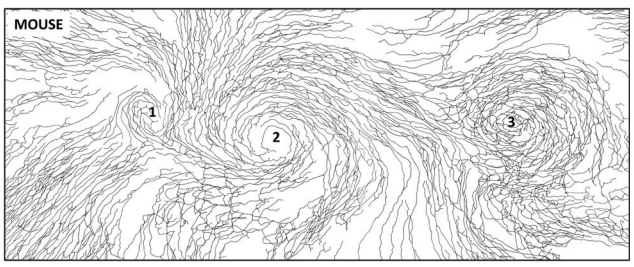

Figure 8. SNP in a C57BL/6 mouse cornea with three separate, closely spaced spirals. The spiral closest to the apex (toward *left* of diagram) rotates clockwise, whereas the other two spirals rotate counterclockwise. The area illustrated is 1.5 × 0.6 mm.

Table 2. Mammalian SNP Patterns

SNP Pattern	Species	References
Whorl-like (spiral)	Mouse	3, 17, 25–37, *
	Rat	22, 41, 42, *
	Guinea Pig	*
	Dog	*
	Cat	51
	Macaque	43, *
	Human	2, 21, 44–50, 63, 70, 71
Horizontal/longitudinal	Rabbit	74, *
	Cow	*
Centrifugal radiation	Pig	*
Random; disorganized	Mole	32

* Present study.

Investigative Ophthalmology & Visual Science

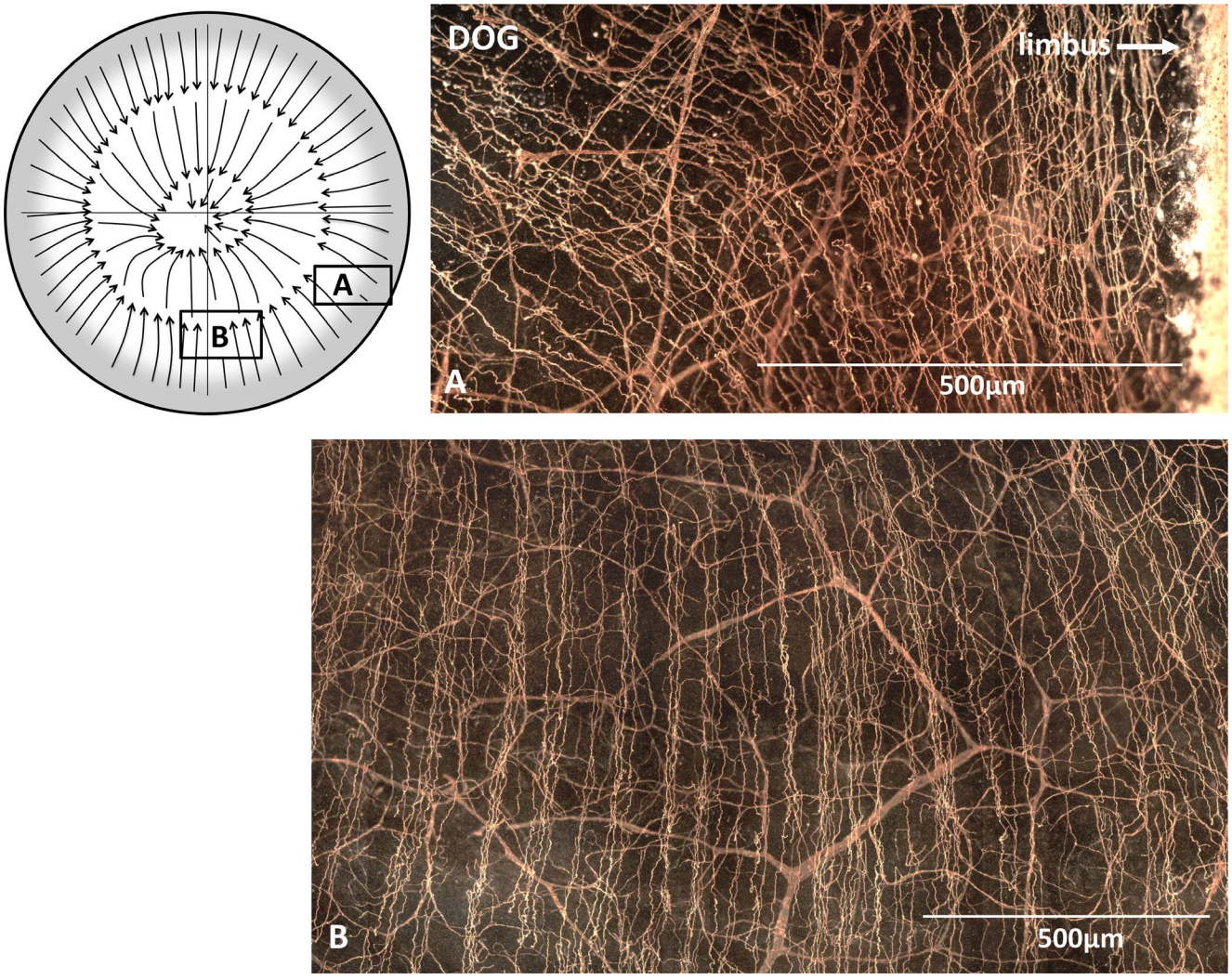

Figure 9. Centripetal organization of the dog SNP. The portions of the SNP photographed in **A** and **B** are indicated by the *inset boxes* in the orientation diagram. (**A**) In the inferonasal quadrant, SNFs often course initially parallel to the limbus, but then change direction and sweep toward the corneal apex. (**B**) SNFs in the peripheral cornea course centripetally toward the central cornea as a regular network of radially directed or gently arching fibers.

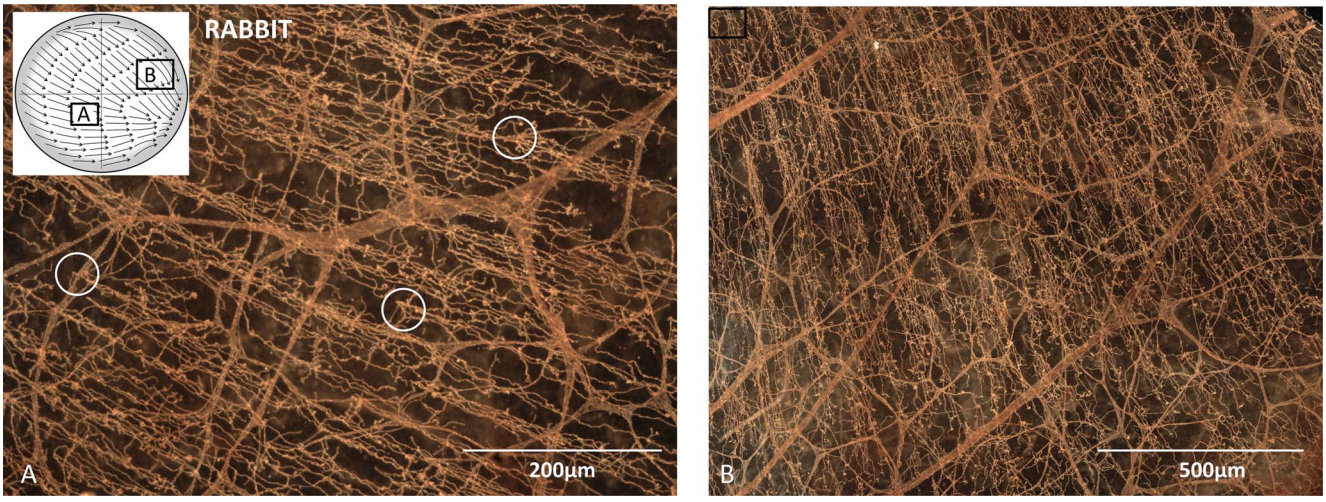

Figure 10. Morphology of the rabbit corneal SNP. The regions of the SNP shown in **A** and **B** are indicated by the *inset boxes* in the orientation diagram. SNFs in all regions of the rabbit cornea radiate uniformly toward the inferonasal limbus. The *circles* in **A** show representative examples of SNF fibers originating from underlying stromal nerves.

Investigative Ophthalmology & Visual Science

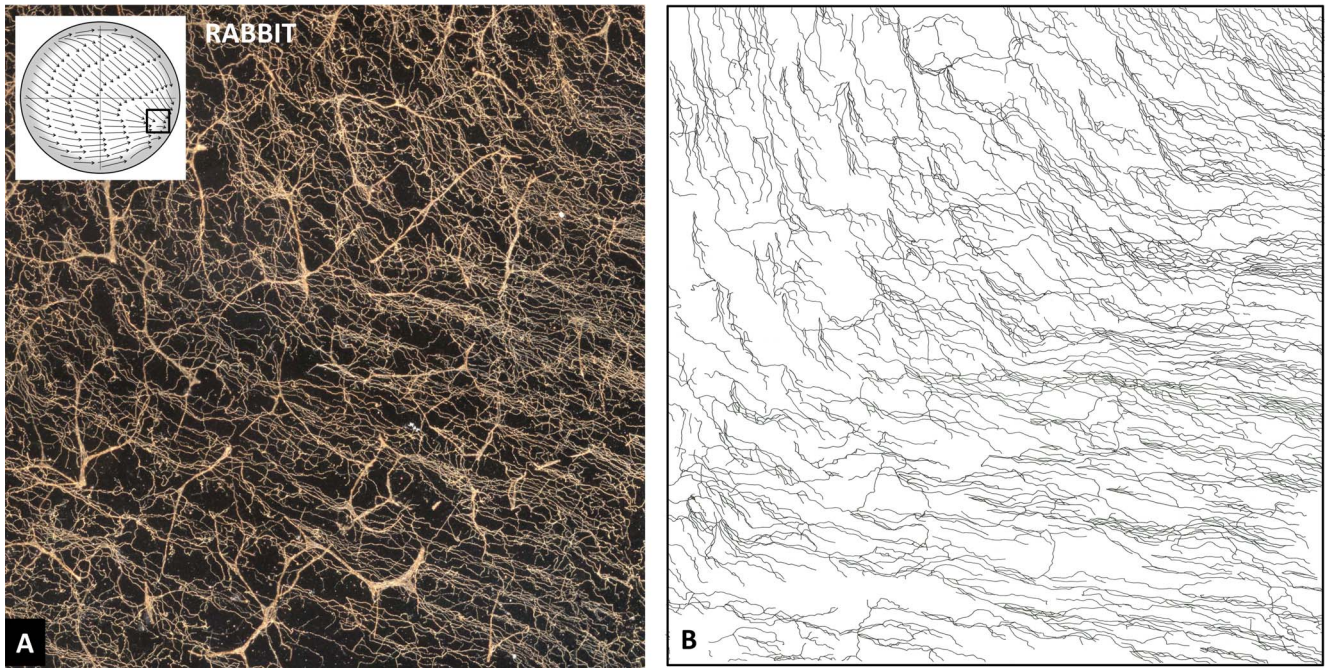

FIGURE 11. SNFs in the perilimbal region of the rabbit inferonasal quadrant (*boxed area* in *inset*). (**A**) Corneal nerves as seen under darkfield optics in the light microscope. (**B**) *Line drawing* made with a drawing tube attachment of the identical area shown in **A**, depicting only the SNFs. The *line drawing* reveals to greater advantage the abrupt change in directional orientation made by the SNFs in this region as they approach the inferonasal limbus. The area illustrated in these figures is 1.0 mm^2.

suggest that the SNF whorl develops prior to, and might thus be independent of, epithelial cell dynamics. Alternatively, homologous whorl-like patterns of corneal epithelial cells and SNFs might respond to similar external guidance cues but on slightly different timetables.[31]

The genetic and molecular mechanisms that govern the formation of the SNP whorl pattern obviously allow for some degree of randomness, since minor variations of the prototypical architectural pattern are common. These variants have been best documented in the mouse and rat corneas, for which the most data are available, and include interanimal variability in apical patterns of SNF convergence, differences in direction of whorl rotation, location of the center of the whorl relative to the corneal apex, and number of whorls per cornea.[3,36,51] Of special interest, approximately 20% of Swiss Webster mouse corneas,[3] and a very small percentage of C57/B6 mouse corneas (present study) contain multiple periapical spirals. The latter observations extend prior reports of significant strain-specific differences in mouse SNP anatomy.[17,69]

Whorl-like patterns of SNFs occur also in human corneas. Since the first description almost three decades ago,[70] human SNF inferonasal whorls have been documented by both IVCM[24,46,47,49,63,71] and ex vivo IHC staining of donor corneas.[2,21,44] The center of the SNF whorl in human corneas is morphologically less distinct and more anastomotic compared with most other mammalian SNP spirals, and both clockwise and counterclockwise whorls have been well documented.[2,21] Curiously, IVCM imaging studies of the human inferonasal whorl report almost exclusively clockwise rotational whorls. Out of 20 total whorl formations described or illustrated in the clinical literature, 19 rotate clockwise[10,24,45–48,50,71,72] and only one rotates counterclockwise.[73] It is possible that the IVCM data are skewed by the relatively small number of corneas examined per study or by author bias to publish images of the most "typical" rotational pattern. The highly characteristic appearance and relatively consistent location of the human inferonasal whorl[2,21,46] makes it an ideal anatomical landmark for longitudinal IVCM quantification of changes in corneal nerve density and morphology in patients with diabetic peripheral neuropathy and other diseases.[45,48]

Mammals in Which the SNP Does Not Form a Whorl-like Pattern

The results of the present study have shown unambiguously that not all mammalian corneal SNPs are organized into centripetal whorl-like patterns. These observations confirm and extend a previous report of a predominantly horizontal organization of the rabbit SNP,[74] and add novel documentation of an analogous longitudinal pattern in bovine corneas. The centrifugal pattern of the porcine corneal SNP reported here is of special interest as it is the polar opposite of the centripetal organizational scheme seen in most mammalian species. This is, to our knowledge, the first anatomical study of corneal innervation in pigs and is of interest because the pig is a popular animal model for eye research.[75,76] Pigs are genetically more similar to humans than are mice,[77,78] and the biomechanical and optical properties of human and porcine corneas are very similar.[79,80] The unique SNP architectural profiles revealed here in the rabbit, cow, and pig suggest that SNP pattern formation is governed by mechanisms that differ fundamentally from those that dictate the centripetal whorl-like orientation seen in most species. In the absence of additional studies, the mechanisms that govern the development of these unique patterns of corneal innervation remain unknown.

Other Factors That Might Influence SNP Pattern Formation

It has been hypothesized that formation of the inferonasal SNP whorl in human corneas may be influenced in part by shearing

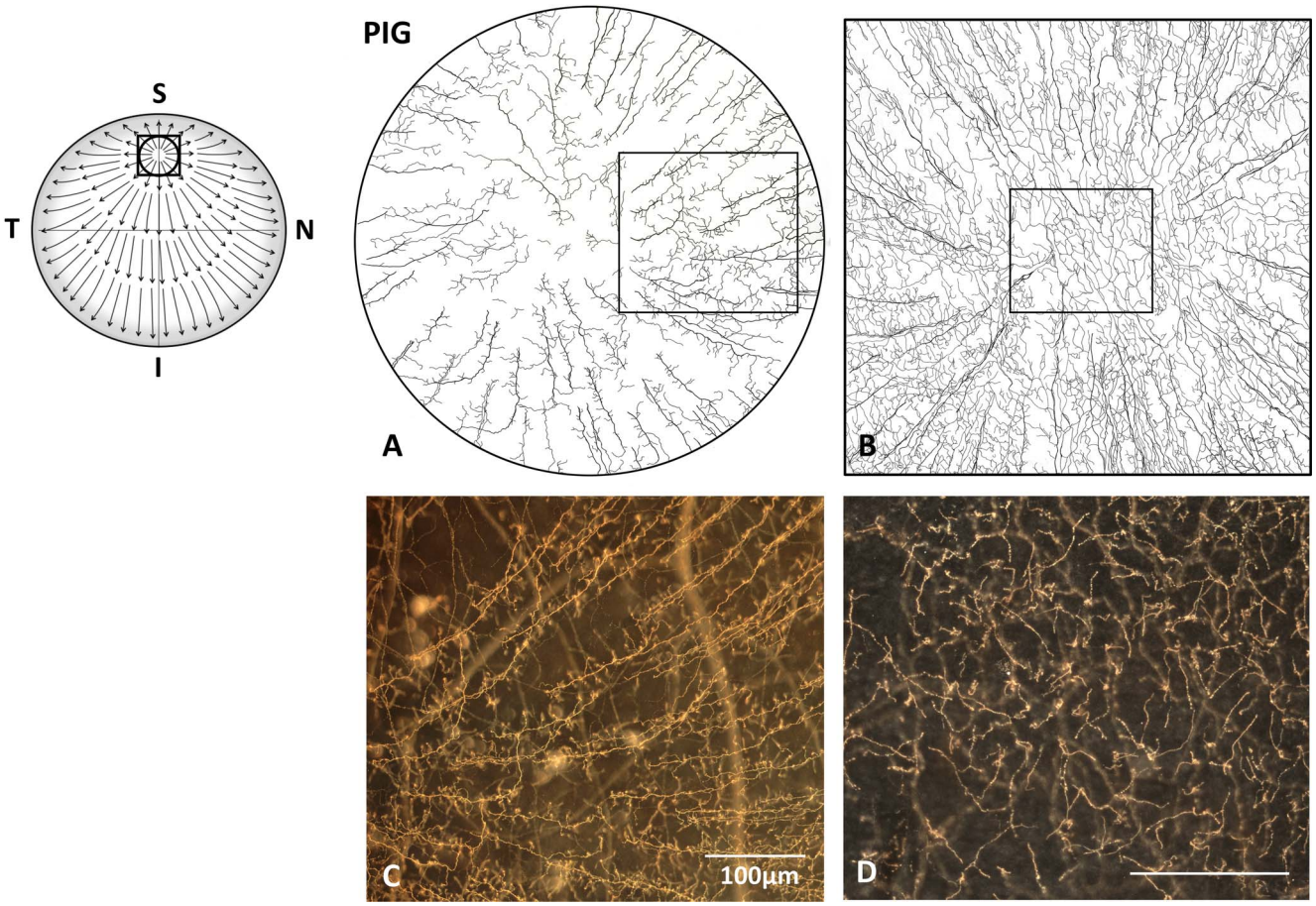

Figure 12. Centrifugal organization of the pig SNP. The locations of the *line drawings* shown in (**A**) and (**B**) are indicated by the *circular* and *square insets*, respectively, in the small orientation figure. (**A, B**) Detailed *line drawings* from two different pig corneas, centered on the SNP "central hub." The areas illustrated in **A** and **B** are 1.0 mm in diameter and 1.0 mm^2, respectively. Note that the SNF densities in these two corneas, from different pigs of unknown ages, are noticeably different. (**C**) Darkfield photomicrograph of centrifugally directed SNFs in the area outlined by the *inset box* in **A**. (**D**) Nerve terminals in the corneal epithelium overlying the area outlined by the *inset box* in **B**. Note that the epithelium overlying the central hub is densely innervated, despite the absence in this area of organized, centrifugally directed SNFs. The calibration bars in **C** and **D** are 100 µm for both figures. S, superior; N, nasal; I, inferior, T, temporal.

or frictional forces exerted on the ocular surface associated with blinking.[46] During blinking, the upper eyelid moves downward and the lower eyelid moves upward and nasally to meet ~2 to 3 mm inferior to the horizontal meridian[81] (i.e., at about the level of the SNP vortex), and simultaneously the eye rotates nasally and inferiorly.[82–84] There is currently no direct evidence to support this intriguing hypothesis, and the presence of prominent inferonasal whorls in animals that blink infrequently (mice, rats, cats) and/or that sleep with their eyelids open (guinea pigs) would seem contrary to this mechanism.[85,86] In human corneas, it has been shown that positive and negative mechanical pressures exerted by orthokeratology (OK) lenses,[47] and stretching pressures associated with advanced keratoconus[87,88] are sufficient to change the SNF orientation and produce distinctive SNP patterns; however, these pressures are considerably greater than the negligible sheering forces that occur during blinking.

The third eyelid, or nictitating membrane, is a mobile protective structure found in many mammals. Contraction of the retractor bulbi muscle causes the eyeball to retract into the orbit and allows the third eyelid to sweep passively across the ocular surface in a nasomedial to dorsolateral direction.[89] Early in the course of this investigation, the authors speculated that shearing forces caused by sweeping movements of the third eyelid over the cornea, in addition to putative neurotrophic factors released into the inferior conjunctival sac by third eyelid glandular secretions, might contribute to the nasomedial directional preference of SNFs in rabbit and cow eyes. However, the absence of comparable longitudinal patterns of SNFs in other mammals with prominent third eyelids, such as the dogs and pigs examined in the current study, and cats,[51] argues against a consistent role of the nictitating membrane in SNP pattern formation.

The results of this study, and of prior investigations, provide no evidence that structural or mechanical factors related to corneal size, shape, radius of curvature, thickness, or other physical attributes play a significant role in SNF pattern formation. For example, animals with large ovoid- or elliptical-shaped corneas are almost equally likely to exhibit whorl-like (cat, dog, macaque, human) or nonwhorl-like (rabbit, cow, pig) SNP patterns. Similarly, in animals that possess prominent spiral-like SNP patterns, the spirals are morphologically indistinguishable in animals with small, nearly spherical, steep and strongly curved corneas (mice and rats), and animals with large, elliptical (horizontal diameter > vertical diameter) and flatter corneas (cats and macaques).

Finally, it is interesting to note that moles, subterranean animals with small eyes that have adapted to life in the dark, lack a well-organized corneal innervation and instead possess sparse, randomly organized corneal nerves that mimic the

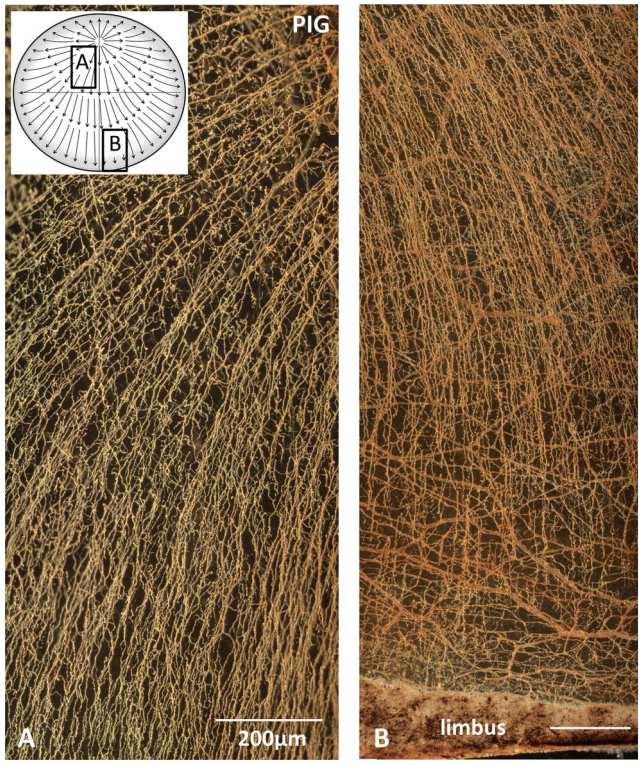

FIGURE 13. Darkfield photomicrographs of the periapical (**A**) and peripheral (**B**) regions of the pig SNP. In all regions of the pig cornea, densely packed, parallel arrays of long, curvilinear SNFs course centrifugally, away from the superior central hub, toward the limbus. Calibration bar is 200 μm for both figures.

immature nerve pattern seen in early postnatal mouse corneas.[32] Because mole eyelids are either fused (Iberian moles) or presumed to be tightly closed during underground activities (European moles), the corneas are rarely exposed to the environment and may lack some essential signal permissive to continued maturation of its rudimentary innervation. In neonatal mice and rats, the developmental timepoint around which immature subbasal fibers begin to first exhibit "adult-like" characteristics, such as elongation and uniform directional orientation, corresponds closely with eyelid opening,[3,90] suggesting that eyelid opening might be an important trigger for continued SNP maturation. It might be concluded that while a dense, highly organized corneal innervation is a physiologic requirement in terrestrial animals to promote ocular surface maintenance and protective blinking, in subterranean animals with fused or closed eyelids a robust corneal innervation might not be needed.[32]

Neurotrophic Influence of the Corneoscleral Limbus

The results of the present study have revealed that many mammalian SNFs and intraepithelial terminals in the extreme peripheral cornea orient preferentially toward the corneoscleral limbus (Fig. 14). It is tempting to speculate that the nerves are attracted in that direction by limbus-derived neurotrophic factors or other external forces, and that these signals are strong enough to antagonize the fundamental directional orientation mechanism. A comparable phenomenon has been described in wounded rabbit corneas; following the creation of a central epithelial injury, wound-derived trophic factors cause regenerating SNFs to elongate preferentially toward the wound

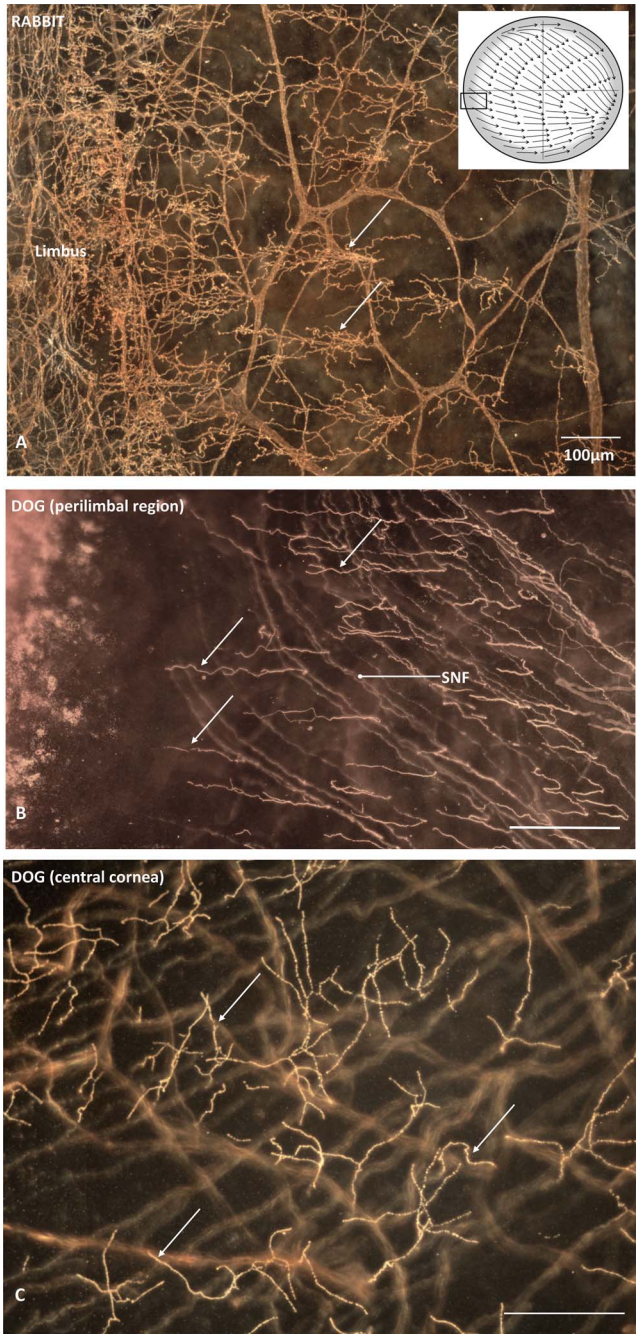

FIGURE 14. Rabbit SNFs (**A**, *arrows*) and dog epithelial terminals (**B**, *arrows*) in the peripheral cornea often orient preferentially toward the corneoscleral limbus. (**C**) Epithelial nerve terminals (*arrows*) elsewhere in the dog cornea do not exhibit a directional preference and are randomly oriented. Calibration bars are 100 μm in all three figures.

margin and thereby deviate, often by as much as 180 degrees, from their normal directional orientation.[74]

Return of SNP Architectural Pattern After Corneal Injuries

It is not known if the same factors that control SNP pattern formation in the developing cornea also direct the return of SNP architecture after corneal injuries. Studies of corneal nerve regeneration in mice have shown that a central whorl-like pattern of the SNP returns by approximately 28 days

postwounding, albeit at a significantly reduced nerve fiber density.[26,37,40,51] Comparable observations in human corneas are extremely limited. Stachs et al.[24] were unable to detect a subbasal whorl pattern in any cornea up to 2 years post-LASIK or 54 months after penetrating keratoplasty, suggesting that in human eyes, the factors that direct SNP pattern formation developmentally are lacking or inadequate to direct reformation of normal corneal SNP architecture after corneal surgery or injury in adults.[24] Factors that enhance or inhibit SNF regeneration after corneal wounding[10,26,91,92] and the dynamics of SNF elongation, regeneration, and sprouting after different types of corneal injuries[22–24,27,93] and following biosynthetic implantation[94] are currently areas of intense investigation.

Summary and Conclusions

The results of this study have demonstrated three highly distinct patterns of SNF organization in the mammalian cornea. It is not known whether the different SNP patterns shown here have physiological significance. It might be that a particular pattern of SNF orientation is needed for a specific functional or anatomic requirement that has yet to be elucidated for any given species. It is tempting to speculate that each of the animal corneas examined in this study has developed a configuration of SNFs that is optimized for that species and that each pattern is uniquely adapted to blanket the dome-shaped corneal surface with a uniformly dense sensory innervation that serves essential sensory, homeostatic, and reflex functions. It is worth emphasizing that despite the intriguing interspecies differences in SNP pattern formation reported here, the corneal innervation in all eight mammals nevertheless share similar foundational blueprints. In every case, stromal nerve fibers give rise to a dense monolayer of SNFs that course parallel to one another, with occasional anastomotic interconnections, within the basal epithelial cell layer. The SNFs, in turn, give rise to an extraordinarily dense network of suprabasal epithelial nerve terminals. Studies in human and animal corneas have shown that epithelial innervation density and sensitivity are, in all mammals, highest in the central cornea, suggesting that each of the three SNP patterns revealed here, regardless of predominant SNF direction orientation, is designed appropriately to provide comparable central-to-peripheral gradients of corneal nerve terminal density and sensitivity.

Finally, it is worth noting that primate corneas are innervated predominantly, if not exclusively, by trigeminal sensory nerves; however, it is estimated that other mammalian corneas, specifically the rabbit, cat and guinea pig, receive upwards of 10% to 15% of their innervation from sympathetic nerves.[95–97] The remarkably uniform SNP pattern seen here in the rabbit and guinea pig, and in a prior study of cat corneas,[51] suggests that genetic, environmental, or molecular factors that determine the development of a particular SNF pattern exert their effects similarly on corneal sensory and sympathetic nerves. Although sensory and sympathetic nerve fibers have distinct neurochemical signatures and, perhaps, different nerve terminal morphologies, they are morphologically indistinguishable within the SNP.

Acknowledgments

Supported by Summer Research Internship funding from Indiana University School of Medicine-Northwest-Gary (C.M.), National Institutes of Health Grants R01NS097221 (J.L.M) and U42OD013117 to support the macaque breeding colony (J.L.M)

Disclosure: **C. Marfurt**, None; **M.C. Anokwute**, None; **K. Fetcko**, None; **E. Mahony-Perez**, None; **H. Farooq**, None; **E. Ross**, None; **M.M. Baumanis**, None; **R.L. Weinberg**, None; **M.E. McCarron**, None; **J.L. Mankowski**, None

References

1. Muller LJ, Marfurt CF, Kruse F, Tervo TM. Corneal nerves: structure, contents and function. *Exp Eye Res*. 2003;76:521–542.
2. Marfurt CF, Cox J, Deek S, Dvorscak L. Anatomy of the human corneal innervation. *Exp Eye Res*. 2010;90:478–492.
3. He J, Bazan HE. Neuroanatomy and neurochemistry of mouse cornea. *Invest Ophthalmol Vis Sci*. 2016;57:664–674.
4. Cajal S. *Texture of the Nervous System of Man and the Vertebrates*. 1st ed. New York: Springer-Verlag Wien; 1999.
5. Klein E. On the termination of the nerves in the mammalian cornea. *Quart J Microscop Sci*. 1880;LXXX:459–475.
6. Muller LJ, Vrensen GF, Pels L, Cardozo BN, Willekens B. Architecture of human corneal nerves. *Invest Ophthalmol Vis Sci*. 1997;38:985–994.
7. Muller LJ, Pels L, Vrensen GF. Ultrastructural organization of human corneal nerves. *Invest Ophthalmol Vis Sci*. 1996;37:476–488.
8. Yang AY, Chow J, Liu J. Corneal innervation and sensation: the eye and beyond. *Yale J Biol Med*. 2018;91:13–21.
9. Patel DV, McGhee CN. In vivo confocal microscopy of human corneal nerves in health, in ocular and systemic disease, and following corneal surgery: a review. *Br J Ophthalmol*. 2009;93:853–860.
10. Cruzat A, Qazi Y, Hamrah P. In vivo confocal microscopy of corneal nerves in health and disease. *Ocul Surf*. 2017;15:15–47.
11. Shaheen BS, Bakir M, Jain S. Corneal nerves in health and disease. *Surv Ophthalmol*. 2014;59:263–285.
12. Bandeira F, Yusoff NZ, Yam GH, Mehta JS. Corneal re-innervation following refractive surgery treatments. *Neural Regen Res*. 2019;14:557–565.
13. Labbe A, Liang H, Martin C, Brignole-Baudouin F, Warnet JM, Baudouin C. Comparative anatomy of laboratory animal corneas with a new-generation high-resolution in vivo confocal microscope. *Curr Eye Res*. 2006;31:501–509.
14. Kafarnik C, Fritsche J, Reese S. Corneal innervation in mesocephalic and brachycephalic dogs and cats: assessment using in vivo confocal microscopy. *Vet Ophthalmol*. 2008;11:363–367.
15. Ledbetter EC, Scarlett JM. In vivo confocal microscopy of the normal equine cornea and limbus. *Vet Ophthalmol*. 2009;12(suppl 1):57–64.
16. Reichard M, Hovakimyan M, Wree A, et al. Comparative in vivo confocal microscopical study of the cornea anatomy of different laboratory animals. *Curr Eye Res*. 2010;35:1072–1080.
17. Reichard M, Weiss H, Poletti E, et al. Age-related changes in murine corneal nerves. *Curr Eye Res*. 2016;41:1021–1028.
18. Simsek C, Kojima T, Nagata T, Dogru M, Tsubota K. Changes in murine subbasal corneal nerves after scopolamine-induced dry eye stress exposure. *Invest Ophthalmol Vis Sci*. 2019;60:615–623.
19. Oakley JD, Russakoff DB, McCarron ME, Weinberg RL, Izzi JM, Mankowski JL. Deep learning-based analysis of macaque corneal sub-basal nerve fibers in confocal microscopy images. *bioRxiv*. 2019;758433.
20. Wang C, Fu T, Xia C, Li Z. Changes in mouse corneal epithelial innervation with age. *Invest Ophthalmol Vis Sci*. 2012;53:5077–5084.
21. He J, Bazan NG, Bazan HE. Mapping the entire human corneal nerve architecture. *Exp Eye Res*. 2010;91:513–523.

22. Hegarty DM, Hermes SM, Morgan MM, Aicher SA. Acute hyperalgesia and delayed dry eye after corneal abrasion injury. *Pain Rep*. 2018;3:e664.
23. Al-Aqaba MA, Otri AM, Fares U, Miri A, Dua HS. Organization of the regenerated nerves in human corneal grafts. *Am J Ophthalmol*. 2012;153:29–37.
24. Stachs O, Zhivov A, Kraak R, Hovakimyan M, Wree A, Guthoff R. Structural-functional correlations of corneal innervation after LASIK and penetrating keratoplasty. *J Refract Surg*. 2010;26:159–167.
25. Downie LE, Naranjo Golborne C, Chen M, et al. Recovery of the sub-basal nerve plexus and superficial nerve terminals after corneal epithelial injury in mice. *Exp Eye Res*. 2018;171: 92–100.
26. Pajoohesh-Ganji A, Pal-Ghosh S, Tadvalkar G, Kyne BM, Saban DR, Stepp MA. Partial denervation of sub-basal axons persists following debridement wounds to the mouse cornea. *Lab Invest*. 2015;95:1305–1318.
27. Yu CQ, Zhang M, Matis KI, Kim C, Rosenblatt MI. Vascular endothelial growth factor mediates corneal nerve repair. *Invest Ophthalmol Vis Sci*. 2008;49:3870–3878.
28. Barrett JE, Wells DC, Conrad GW. Pretreatment methods to improve nerve immunostaining in corneas from long-term fixed embryonic quail eyes. *J Neurosci Methods*. 1999;92: 161–168.
29. Yu CQ, Rosenblatt MI. Transgenic corneal neurofluorescence in mice: a new model for in vivo investigation of nerve structure and regeneration. *Invest Ophthalmol Vis Sci*. 2007; 48:1535–1542.
30. Yuasa M, Kobayashi A, Yokogawa H, Sugiyama K. In vivo laser confocal microscopic analysis of murine cornea and lens microstructures. *Ophthalmic Surg Lasers Imaging*. 2008;39: 391–396.
31. Leiper LJ, Ou J, Walczysko P, et al. Control of patterns of corneal innervation by Pax6. *Invest Ophthalmol Vis Sci*. 2009;50:1122–1128.
32. Carmona FD, Ou J, Jimenez R, Collinson JM. Development of the cornea of true moles (Talpidae): morphogenesis and expression of PAX6 and cytokeratins. *J Anat*. 2010;217:488–500.
33. Li Z, Burns AR, Han L, Rumbaut RE, Smith CW. IL-17 and VEGF are necessary for efficient corneal nerve regeneration. *Am J Pathol*. 2011;178:1106–1116.
34. McKenna CC, Lwigale PY. Innervation of the mouse cornea during development. *Invest Ophthalmol Vis Sci*. 2011;52:30–35.
35. Namavari A, Chaudhary S, Sarkar J, et al. In vivo serial imaging of regenerating corneal nerves after surgical transection in transgenic thy1-YFP mice. *Invest Ophthalmol Vis Sci*. 2011; 52:8025–8032.
36. Ivanusic JJ, Wood RJ, Brock JA. Sensory and sympathetic innervation of the mouse and guinea pig corneal epithelium. *J Comp Neurol*. 2013;521:877–893.
37. Reichard M, Hovakimyan M, Guthoff RF, Stachs O. In vivo visualisation of murine corneal nerve fibre regeneration in response to ciliary neurotrophic factor. *Exp Eye Res*. 2014; 120:20–27.
38. Leckelt J, Guimaraes P, Kott A, Ruggeri A, Stachs O, Baltrusch S. Early detection of diabetic neuropathy by investigating CNFL and IENFD in thy1-YFP mice. *J Endocrinol*. 2016;231: 147–157.
39. Kneer K, Green MB, Meyer J, Rich CB, Minns MS, Trinkaus-Randall V. High fat diet induces pre-type 2 diabetes with regional changes in corneal sensory nerves and altered P2X7 expression and localization. *Exp Eye Res*. 2018;175:44–55.
40. Bech F, Gonzalez-Gonzalez O, Artime E, et al. Functional and morphologic alterations in mechanical, polymodal, and cold sensory nerve fibers of the cornea following photorefractive keratectomy. *Invest Ophthalmol Vis Sci*. 2018;59:2281–2292.
41. Dvorscak L, Marfurt CF. Age-related changes in rat corneal epithelial nerve density. *Invest Ophthalmol Vis Sci*. 2008;49: 910–916.
42. Hegarty DM, Hermes SM, Yang K, Aicher SA. Select noxious stimuli induce changes on corneal nerve morphology. *J Comp Neurol*. 2017;525:2019–2031.
43. Dorsey JL, Mangus LM, Oakley JD, et al. Loss of corneal sensory nerve fibers in SIV-infected macaques: an alternate approach to investigate HIV-induced PNS damage. *Am J Pathol*. 2014;184:1652–1659.
44. Al-Aqaba MA, Fares U, Suleman H, Lowe J, Dua HS. Architecture and distribution of human corneal nerves. *Br J Ophthalmol*. 2010;94:784–789.
45. Petropoulos IN, Ferdousi M, Marshall A, et al. The inferior whorl for detecting diabetic peripheral neuropathy using corneal confocal microscopy. *Invest Ophthalmol Vis Sci*. 2015;56:2498–2504.
46. Patel DV, McGhee CN. Mapping of the normal human corneal sub-Basal nerve plexus by in vivo laser scanning confocal microscopy. *Invest Ophthalmol Vis Sci*. 2005;46:4485–4488.
47. Lum E, Golebiowski B, Swarbrick HA. Mapping the corneal sub-basal nerve plexus in orthokeratology lens wear using in vivo laser scanning confocal microscopy. *Invest Ophthalmol Vis Sci*. 2012;53:1803–1809.
48. Utsunomiya T, Nagaoka T, Hanada K, et al. Imaging of the corneal subbasal whorl-like nerve plexus: more accurate depiction of the extent of corneal nerve damage in patients with diabetes. *Invest Ophthalmol Vis Sci*. 2015;56:5417–5423.
49. Edwards K, Pritchard N, Poole C, et al. Development of a novel technique to measure corneal nerve migration rate. *Cornea*. 2016;35:700–705.
50. Kalteniece A, Ferdousi M, Petropoulos I, et al. Greater corneal nerve loss at the inferior whorl is related to the presence of diabetic neuropathy and painful diabetic neuropathy. *Sci Rep*. 2018;8:3283.
51. He J, Pham TL, Bazan HEP. Mapping the entire nerve architecture of the cat cornea. *Vet Ophthalmol*. 2019;22: 345–352.
52. Thoft RA, Friend J. The X, Y, Z hypothesis of corneal epithelial maintenance. *Invest Ophthalmol Vis Sci*. 1983;24:1442–1443.
53. Dua HS, Watson NJ, Mathur RM, Forrester JV. Corneal epithelial cell migration in humans: 'hurricane and blizzard keratopathy'. *Eye (Lond)*. 1993;7:53–58.
54. Dua HS, Gomes JA, Singh A. Corneal epithelial wound healing. *Br J Ophthalmol*. 1994;78:401–408.
55. Dua HS, Singh A, Gomes JA, Laibson PR, Donoso LA, Tyagi S. Vortex or whorl formation of cultured human corneal epithelial cells induced by magnetic fields. *Eye (Lond)*. 1996;10:447–450.
56. Dua HS, Gomes JA. Clinical course of hurricane keratopathy. *Br J Ophthalmol*. 2000;84:285–288.
57. Collinson JM, Morris L, Reid AI, et al. Clonal analysis of patterns of growth, stem cell activity, and cell movement during the development and maintenance of the murine corneal epithelium. *Dev Dyn*. 2002;224:432–440.
58. Collinson JM, Chanas SA, Hill RE, West JD. Corneal development, limbal stem cell function, and corneal epithelial cell migration in the Pax6(+/–) mouse. *Invest Ophthalmol Vis Sci*. 2004;45:1101–1108.
59. Song B, Zhao M, Forrester J, McCaig C. Nerve regeneration and wound healing are stimulated and directed by an endogenous electrical field in vivo. *J Cell Sci*. 2004;117: 4681–4690.

Investigative Ophthalmology & Visual Science

60. Iannaccone S, Zhou Y, Walterhouse D, Taborn G, Landini G, Iannaccone P. Three dimensional visualization and fractal analysis of mosaic patches in rat chimeras: cell assortment in liver, adrenal cortex and cornea. *PLoS One*. 2012;7:e31609.
61. Mohammad Nejad T, Iannaccone S, Rutherford W, Iannaccone PM, Foster CD. Mechanics and spiral formation in the rat cornea. *Biomech Model Mechanobiol*. 2015;14:107–122.
62. Stepp MA, Tadvalkar G, Hakh R, Pal-Ghosh S. Corneal epithelial cells function as surrogate Schwann cells for their sensory nerves. *Glia*. 2017;65:851–863.
63. Auran JD, Koester CJ, Kleiman NJ, et al. Scanning slit confocal microscopic observation of cell morphology and movement within the normal human anterior cornea. *Ophthalmology*. 1995;102:33–41.
64. Kuhlemeier C. Phyllotaxis. In: *Current Biology Magazine*. Amsterdam: Elsevier Ltd.; 2017:R882–R887.
65. Samlaska CP, James WD, Sperling LC. Scalp whorls. *J Am Acad Dermatol*. 1989;21:553–556.
66. Wunderlich RC, Heerema NA. Hair crown patterns of human newborns. Studies on parietal hair whorl locations and their directions. *Clin Pediatr (Phila)*. 1975;14:1045–1049.
67. Paul SP. Golden spirals and scalp whorls: nature's own design for rapid expansion. *PLoS One*. 2016;11:e0162026.
68. Nagasaki T, Zhao J. Centripetal movement of corneal epithelial cells in the normal adult mouse. *Invest Ophthalmol Vis Sci*. 2003;44:558–566.
69. Pham TL, Kakazu A, He J, Bazan HEP. Mouse strains and sexual divergence in corneal innervation and nerve regeneration. *FASEB J*. 2019;33:4598–4609.
70. Ueda S, del Cerro M, LoCascio JA, Aquavella JV. Peptidergic and catecholaminergic fibers in the human corneal epithelium. An immunohistochemical and electron microscopic study. *Acta Ophthalmol Suppl*. 1989;192:80–90.
71. Patel DV, McGhee CN. In vivo laser scanning confocal microscopy confirms that the human corneal sub-basal nerve plexus is a highly dynamic structure. *Invest Ophthalmol Vis Sci*. 2008;49:3409–3412.
72. Lagali NS, Allgeier S, Guimaraes P, et al. Wide-field corneal subbasal nerve plexus mosaics in age-controlled healthy and type 2 diabetes populations. *Sci Data*. 2018;5:180075.
73. Lagali NS, Peebo BB, Germundsson J, et al. Laser-scanning in vivo confocal microscopy of the cornea: imaging and analysis methods for preclinical and clinical applications. In: Lagali N, ed. *Confocal Laser Microscopy:Principles and Applications in Medicine, Biology, and the Food Sciences*. London: Intech Open; 2013:52–74.
74. de Leeuw AM, Chan KY. Corneal nerve regeneration. Correlation between morphology and restoration of sensitivity. *Invest Ophthalmol Vis Sci*. 1989;30:1980–1990.
75. Lagali NS, Griffith M, Shinozaki N, Fagerholm P, Munger R. Innervation of tissue-engineered corneal implants in a porcine model: a 1-year in vivo confocal microscopy study. *Invest Ophthalmol Vis Sci*. 2007;48:3537–3544.
76. Choy EP, Cho P, Benzie IF, Choy CK. Dry eye and blink rate simulation with a pig eye model. *Optom Vis Sci*. 2008;85:129–134.
77. Humphray SJ, Scott CE, Clark R, et al. A high utility integrated map of the pig genome. *Genome Biol*. 2007;8:R139.
78. Groenen MA, Archibald AL, Uenishi H, et al. Analyses of pig genomes provide insight into porcine demography and evolution. *Nature*. 2012;491:393–398.
79. Abhari S, Eisenback M, Kaplan HJ, Walters E, Prather RS, Scott PA. Anatomic studies of the miniature swine cornea. *Anat Rec (Hoboken)*. 2018;301:1955–1967.
80. Sanchez I, Martin R, Ussa F, Fernandez-Bueno I. The parameters of the porcine eyeball. *Graefes Arch Clin Exp Ophthalmol*. 2011;249:475–482.
81. Oyster CW. The eyelids and the lacrimal system. In: *The Human Eye Structure and Function*. Sunderland, MA: Sinauer Associates, Inc.; 1999:291–320.
82. Collewijn H, van der Steen J, Steinman RM. Human eye movements associated with blinks and prolonged eyelid closure. *J Neurophysiol*. 1985;54:11–27.
83. Riggs LA, Kelly JP, Manning KA, Moore RK. Blink-related eye movements. *Invest Ophthalmol Vis Sci*. 1987;28:334–342.
84. Bour LJ, Aramideh M, de Visser BW. Neurophysiological aspects of eye and eyelid movements during blinking in humans. *J Neurophysiol*. 2000;83:166–176.
85. Trost K, Skalicky M, Nell B. Schirmer tear test, phenol red thread tear test, eye blink frequency and corneal sensitivity in the guinea pig. *Vet Ophthalmol*. 2007;10:143–146.
86. Blount WP. Studies of the movements of the eyelids of animals: blinking. *Quart J Exp Physiol*. 1927;18:111–125.
87. Patel DV, McGhee CN. Mapping the corneal sub-basal nerve plexus in keratoconus by in vivo laser scanning confocal microscopy. *Invest Ophthalmol Vis Sci*. 2006;47:1348–1351.
88. Al-Aqaba MA, Faraj L, Fares U, Otri AM, Dua HS. The morphologic characteristics of corneal nerves in advanced keratoconus as evaluated by acetylcholinesterase technique. *Am J Ophthalmol*. 2011;152:364–376.e361.
89. Maggs DJ. Third eyelid. In: *Slatter's Fundamentals of Veterinary Ophthamology*. Amsterdam: Elsevier; 2008:151–156.
90. Jones MA, Marfurt CF. Calcitonin gene-related peptide and corneal innervation: a developmental study in the rat. *J Comp Neurol*. 1991;313:132–150.
91. Namavari A, Chaudhary S, Ozturk O, et al. Semaphorin 7a links nerve regeneration and inflammation in the cornea. *Invest Ophthalmol Vis Sci*. 2012;53:4575–4585.
92. Omoto M, Yoshida S, Miyashita H, et al. The semaphorin 3A inhibitor SM-345431 accelerates peripheral nerve regeneration and sensitivity in a murine corneal transplantation model. *PLoS One*. 2012;7:e47716.
93. Chan KY, Jarvelainen M, Chang JH, Edenfield MJ. A cryodamage model for studying corneal nerve regeneration. *Invest Ophthalmol Vis Sci*. 1990;31:2008–2021.
94. Fagerholm P, Lagali NS, Merrett K, et al. A biosynthetic alternative to human donor tissue for inducing corneal regeneration: 24-month follow-up of a phase 1 clinical study. *Sci Transl Med*. 2010;2:46ra61.
95. Laties AM, Jacobowitz D. A comparative study of the autonomic innervation of the eye in monkey, cat, and rabbit. *Anat Rec*. 1966;156:383–395.
96. Marfurt CF, Kingsley RE, Echtenkamp SE. Sensory and sympathetic innervation of the mammalian cornea. A retrograde tracing study. *Invest Ophthalmol Vis Sci*. 1989;30:461–472.
97. Marfurt CF, Ellis LC. Immunohistochemical localization of tyrosine hydroxylase in corneal nerves. *J Comp Neurol*. 1993;336:517–531.

Investigative Ophthalmology & Visual Science